Cross sections for 14-eV e-H_2 resonant collisions: Isotope effect in dissociative electron attachment

R. Celiberto*
Department of Water Engineering and Chemistry, Polytechnic of Bari, I-70125 Bari, Italy and
Institute of Inorganic Methodologies and Plasmas, CNR, I-70125 Bari, Italy

R. K. Janev†
Macedonian Academy of Sciences and Arts, P.O.B 428, 1000 Skopje, Macedonia and
Institute of Energy and Climate Research–Plasma Physics, Forschungszentrum Jülich GmbH Association EURATOM-FZJ, Partner in Trilateral Euregio Cluster, D-52425 Jülich, Germany

J. M. Wadehra‡
Physics Department, Wayne State University, Detroit, Michigan 48202 USA

A. Laricchiuta§
Institute of Inorganic Methodologies and Plasmas, CNR, I-70125 Bari, Italy
(Received 6 April 2011; published 29 July 2011)

The process of dissociative attachment of electrons to molecular hydrogen and its isotopes in the energy range at approximately 14 eV is investigated. The dissociative electron attachment cross sections for all six hydrogen isotopes are calculated over an extended range of electron energies using the local complex potential model with the excited Rydberg $^2\Sigma_g^+$ electronic state of H_2^- acting as the intermediate resonant state. A significant isotope effect in theoretical electron attachment cross sections is observed, in agreement with previous predictions and experimental observations. A two-parameter analytic expression for the cross section is derived from the theory that fits accurately the numerically calculated cross sections for all isotopes. Similarly, an analytic mass-scaling relation is derived from the theory that accurately reproduces the numerically calculated rate coefficients for all isotopes in the 0.1–1000 eV temperature range by using the rate coefficient for the H_2 isotope only. The latter is represented by an analytic fit expression with two parameters only.

DOI: 10.1103/PhysRevA.84.012707 PACS number(s): 34.80.Ht, 52.20.Fs

I. INTRODUCTION

Collision and radiative processes of atomic and molecular hydrogen and their isotopes play an important role in the chemistry of the early Universe, the evolution of stellar objects [1], as well as in the physics and chemistry of laboratory fusion plasmas [2]. A comprehensive modeling of physical properties of these systems requires, therefore, knowledge of the cross sections (or reaction-rate coefficients) of all collision processes involving atomic and molecular hydrogen and their isotopes (neutral or ionized). In this paper we shall investigate the process of dissociative electron attachment (DEA) to molecular hydrogen, H_2, and its five heavier isotopes HD, HT, D_2, DT, and T_2 for electron energies in the vicinity of a 14-eV cross-section peak. As the DEA process in these systems has been the subject of many studies in the past (see below), the present investigation will be focused on the mass-scaling properties of DEA cross section and rate coefficients and on deriving analytic representations for them that are valid in a broad range of their variables (the collision energy and temperature, respectively).

Theoretically, the process of dissociative electron attachment to H_2 (or any of its heavier isotopes) is understood [3] to initiate through the formation of an intermediate resonant state of H_2^- as

$$e + H_2 \rightarrow H_2^- \rightarrow H + H^-. \quad (1)$$

Experimentally, the cross sections for DEA to H_2 and its isotopes show three distinct peaks [4–7] over the electron energy range from 3 to 20 eV. The two peaks at ∼3.75 and 14 eV are observed to be quite sharp while the third peak at ∼10 eV is rather broad. It has been recognized [3–10], that the peaks at ∼3.75 and 10 eV correspond to the formation of $X^2\Sigma_u^+$ and $B^2\Sigma_g^+$ resonant states of H_2^-, which asymptotically dissociate into $H(1s)$ and $H^-(1s^2)$, while the sharp peak at ∼14 eV corresponds to the formation of intermediate $^2\Sigma_g^+$ excited electronic Rydberg state of H_2^-, which dissociates into $H(n = 2)$ and $H^-(1s^2)$. The potential curves of these three resonant states have different characteristics which lead to DEA cross sections that exhibit entirely distinct behaviors as the electron energy is varied. Specifically, the potential curve of the $B^2\Sigma_g^+$ resonant state is purely repulsive while the potential curves of the $X^2\Sigma_u^+$ and the Rydberg $^2\Sigma_g^+$ excited electronic states are attractive in the Franck-Condon region of the ground state of H_2. The attractive nature of the resonant potential curves is responsible for the vertical onset of the DEA cross sections at the threshold [10]. In the following discussion, therefore, our attention will be focused on DEA cross sections at ∼14–17 eV, with the threshold peak arising from the Rydberg $^2\Sigma_g^+$ resonant electronic state. The sharp

*r.celiberto@poliba.it
†r.janev@fz-juelich.de
‡wadehra@wayne.edu
§annarita.laricchiuta@ba.imip.cnr.it

peak at ∼14 eV corresponds to the vertical onset of the DEA cross sections at threshold [10].

In the following section we discuss the dissociative attachment cross sections involving the excited $^2\Sigma_g^+$ resonant state for all six hydrogen isotopes as a function of incident electron energy, and derive a general analytic expression for the cross section in which its mass and energy dependences are separated. In Sec. III a similar analytic representation of the isotope effect in DEA process is derived for the rate coefficient. In Sec. IV we give our discussion and conclusions.

II. CROSS-SECTION RESULTS AND ANALYTICAL FITS

The cross sections for the above-mentioned DEA processes are calculated within the local resonant potential model by adopting the same input data (resonant potential and level widths) and using the same numerical procedure as used in our previous calculations with $^2\Sigma_g^+$ excited electronic Rydberg resonant state [11]. The DEA cross section can be expressed as [3]

$$\sigma(E) = 2\pi^2 \frac{m_e}{M} \frac{K}{k_i} \lim_{R\to\infty} |\xi(R)|^2 , \tag{2}$$

where $\xi(R)$ is the local nuclear wave function for the resonant state, $E = \hbar^2 k_i^2/(2m_e)$ is the incident electron energy, m_e is the electron mass, M is the reduced mass of the nuclei, and K is the outgoing negative-ion momentum.

The calculated DEA cross sections for all six isotopes, with the molecules in their lowest vibrational level ($v_i = 0$), are shown in Fig. 1 for the Rydberg $^2\Sigma_g^+$ excited electronic resonant state as a function of the incident electron energy. The small crosses on the energy axis indicate the threshold energy for each isotope. The isotope effect is evident: The attachment cross section decreases with increasing the mass of the isotope. Furthermore, the peak value of the cross section σ_{peak} occurs at the threshold so that σ_{peak} is the same as $\sigma(E_{\text{th}})$, the cross section at the threshold. Table I provides the values of

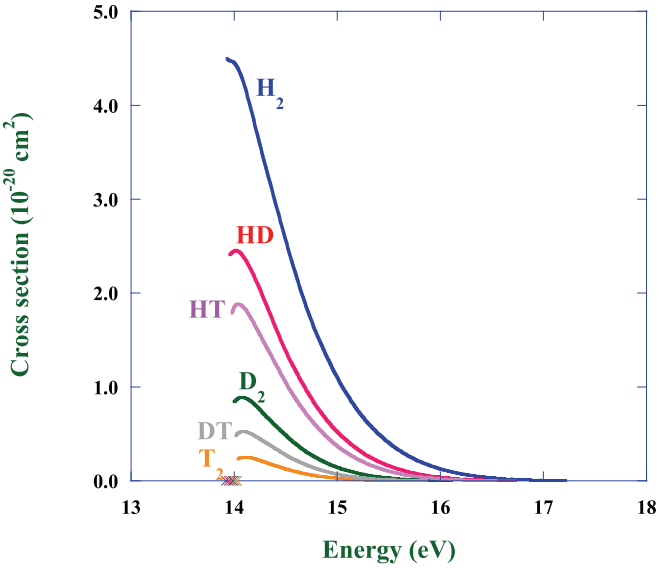

FIG. 1. (Color online) DEA cross sections for all the six isotopes of H_2 occurring through the Rydberg $^2\Sigma_g^+$ excited electronic resonant state.

TABLE I. Threshold energy and the corresponding peak DEA cross sections for all six isotopes of H_2 for the Rydberg $^2\Sigma_g^+$ resonant state.

Isotope[a] I_2	M_{I_2}/M_{H_2}	E_{th} (eV)	σ_{peak} (10^{-20} cm^2)
H_2	1	13.93	4.4955
HD	1.33	13.96	2.4086
HT	1.50	13.98	1.7879
D_2	2.00	14.00	0.84509
DT	2.40	14.02	0.48193
T_2	3.00	14.04	0.23363

[a]Here and in Tables II, I_2 denotes conventionally a homonuclear or heteronuclear molecular isotope.

threshold energy E_{th} and the corresponding peak cross section σ_{peak} for all six isotopes of H_2 for the excited $^2\Sigma_g^+$ Rydberg resonance.

In order to understand the physical behavior of the cross-section curves, we assume a narrow resonance and use the semiclassical Wentzel-Kramers-Brillouin (WKB) approximation to express the DEA cross sections as [3] (see also Refs. [12] and [13])

$$\sigma(E) = \sigma_{\text{cap}}(E) e^{-\int_{R_c}^{R_s} \frac{\Gamma(R)}{\hbar} \frac{dR}{v(R)}} , \tag{3}$$

where R_c is the capture radius, R_s is the stabilization point, and $v(R)$ is the radial velocity with which the nuclei separate along the H_2^- potential curve. R_c corresponds to the internuclear distance at which the electron is captured to form the resonance and R_s corresponds to the crossing point of the potential curves of the neutral H_2 molecule and the resonant H_2^- state. For internuclear separations larger than R_s, electron autodetachment is no longer energetically possible, the resonance width vanishes, and the nuclei separate out into an ion-atom pair. The first factor σ_{cap} in Eq. (3) is interpreted as the cross section for resonance formation by electron capture. An explicit expression for σ_{cap} using the semiclassical WKB approximation is given as [3]

$$\sigma_{\text{cap}}(E) = \frac{\pi^{3/2}}{k_i^2} \frac{\Gamma_c(R_c)}{W_1 a} \exp\left[-\frac{\{E - V^-(R_0)\}^2 - \Gamma^2(R_0)/4}{W_1{}^2 a^2} \right] , \tag{4}$$

where Γ_c is the partial width for electron capture that depends on the in- and outgoing electron wave functions, R_0 is the ground-state equilibrium distance, $\Gamma(R)$ is the resonance width, and a is the vibrational amplitude of the nuclear wave function. We note that in deriving Eq. (4) the so-called *reflection approximation* has been used for the Franck-Condon overlap integral of the initial- and final-state nuclear wave functions at the classical turning point R_c. Further, $V^-(R)$ is the resonant state potential and W_1 is its slope at $R = R_c$. The exponential factor in Eq. (3) is the survival probability of the system in the resonant state against autodetachment. This survival factor is mass dependent. If it is approximated as $\exp(-\bar{\Gamma}\tau/\hbar)$, where $\bar{\Gamma}$ is the average width of the resonance, then the time τ needed by the nuclei to separate from R_c to R_s is obviously directly proportional to $M^{1/2}$. The exponential

dependence of the DEA cross section on the reduced mass of dissociating molecule expresses its strong isotope dependence and was predicted by Bardsley *et al.* [12] and Demkov [13]. The DEA cross section can now be written as

$$\sigma(E) = \sigma_{\rm cap}(E) e^{-c\sqrt{M}}, \tag{5}$$

where c is a mass-independent constant. In order to determine the dependence of $\sigma_{\rm cap}$ on the reduced mass, we first note that the expression in Eq. (3) was obtained in the WKB approximation by assuming a small resonance width and a repulsive resonance potential curve $V^-(R)$. However, the potential curve of $^2\Sigma_g^+$ resonant state, considered in the present paper, is slightly attractive in the Franck-Condon region of the initial $v_i = 0$ vibrational wave function. In such a case, the cross-section curve is calculated in the same way as for a repulsive resonance curve and is simply deleted below the threshold energy $E_{\rm th}$, resulting in the vertical onset or peak of the DEA cross section at the threshold [10]. It is reasonable, therefore, to tentatively replace $V^-(R_0)$, which is just below the dissociative attachment threshold, with the threshold energy $E_{\rm th}$ in $\sigma_{\rm cap}$ of Eq. (4). Also, in expression (4) for $\sigma_{\rm cap}(E)$, the isotope mass appears through a, the vibrational amplitude of nuclear motion, and through $E_{\rm th}$. As seen in Fig. 1, the relative variation of $E_{\rm th}$ with the isotope mass is quite small. Furthermore, because of the compactness of the nuclear wave function of the $v_i = 0$ level, the vibrational amplitude a of the nuclear motion can be approximated by the vibrational amplitude of a linear harmonic oscillator, which for the lowest level is [14]

$$a = \left(\frac{\hbar}{\omega M}\right)^{1/2}. \tag{6}$$

Since the forces that isotopes of different masses experience are the same, the frequency of oscillations ω is inversely proportional to $\sqrt{M}$. Equation (4) can then be written as

$$\sigma_{\rm cap}(E) = \frac{AM^{1/4}}{E} \exp\left[-\gamma\left(\frac{M_{I_2}}{M_{H_2}}\right)^{1/2}\{E - E_{\rm th}\}^2\right], \tag{7}$$

where A and γ are two energy-independent constants. For later convenience, the isotope mass is explicitly expressed in units of the mass of H_2 in the exponent. The constant A includes the term $\exp\left[\gamma\sqrt{M}\Gamma^2(R_0)/4\right]$. Due to the small value for $\Gamma(R_0 = 1.4$ a.u.) ($\approx$0.05 eV, see Ref. [15]), the value of this exponential for the Rydberg resonance is close to one, independently of the isotope mass. Finally, using the dimensionless quantity $x = E/E_{\rm th}$, the expression for the dissociative electron attachment cross section, showing explicitly the mass and energy dependence, takes the form

$$\begin{aligned}\sigma(x) &= \sigma_{\rm cap} e^{-c\sqrt{M}} \\ &= \frac{AM^{1/4}e^{-c\sqrt{M}}}{E_{\rm th}x} \exp\left[-\gamma\left(\frac{M_{I_2}}{M_{H_2}}\right)^{1/2} E_{\rm th}^2\{x-1\}^2\right].\end{aligned} \tag{8}$$

Now, for $E = E_{\rm th}$ or $x = 1$, Eq. (8) reduces to

$$\sigma(1) = \frac{AM^{1/4}e^{-c\sqrt{M}}}{E_{\rm th}} = \sigma_{\rm peak}, \tag{9}$$

TABLE II. $R(I_2,I_2')$ obtained from the calculated peak cross sections and from the mass ratio [Eq. (11)] for the Rydberg resonance $^2\Sigma_g^+$.

Isotopes I_2,I_2'	$\frac{\ln[\sigma_{\rm peak}(I_2)/\sigma_{\rm peak}(H_2)]}{\ln[\sigma_{\rm peak}(I_2')/\sigma_{\rm peak}(H_2)]}$	$\frac{\sqrt{M_{I_2}/M_{H_2}}-1}{\sqrt{M_{I_2'}/M_{H_2}}-1}$
HD, HT	0.6768	0.6819
HD, D_2	0.3734	0.3700
HD, DT	0.2795	0.2791
HD, T_2	0.2110	0.2094
HT, D_2	0.5517	0.5426
HT, DT	0.4129	0.4092
HT, T_2	0.3118	0.3070
D_2, DT	0.7485	0.7542
D_2, T_2	0.5652	0.5658
DT, T_2	0.7551	0.7502

which allows to rewrite Eq. (8) as

$$\sigma(x) = \frac{\sigma_{\rm peak}}{x} \exp\left[-\gamma\left(\frac{M_{I_2}}{M_{H_2}}\right)^{1/2} E_{\rm th}^2\{x-1\}^2\right]. \tag{10}$$

Using Eq. (9) the following relation can be obtained [16]:

$$R(I_2,I_2') = \frac{\ln\left[\sigma_{\rm peak}(I_2)/\sigma_{\rm peak}(H_2)\right]}{\ln\left[\sigma_{\rm peak}(I_2')/\sigma_{\rm peak}(H_2)\right]} \approx \frac{\sqrt{M_{I_2}/M_{H_2}}-1}{\sqrt{M_{I_2'}/M_{H_2}}-1}, \tag{11}$$

where I_2 and I_2' are two different heavier isotopes of H_2 (including the heteronuclear species) and $\sigma_{\rm peak} = \sigma(E_{\rm th})$, where $E_{\rm th}$ is the dissociative attachment threshold energy for the specified isotope. In order to verify the validity of Eq. (11) in our systems, we show in Table II the ratio $R(I_2,I_2')$ evaluated using the calculated peak cross sections $\sigma_{\rm peak}$ and using the mass ratios M_{I_2}/M_{H_2} for all possible pairs of isotopes. The agreement is quite good, suggesting that the various approximations that were made in arriving at Eq. (10) are reasonable. In fact, Eq. (10) is valid for all six isotopes of H_2 with only one unknown quantity γ. If γ is determined using cross sections for one of the isotopes, say, H_2, then the cross sections for the remaining five isotopes are automatically fitted by Eq. (10). The fitting of DEA cross sections, obtained in this manner, was found to be quite good for all isotopic variants. However, even better fitting results can be obtained if we add in Eq. (10) a further parameter, q, such that $\{x-1\}^2$ is replaced by $\{x-1\}^q$, i.e.,

$$\sigma(x) = \frac{\sigma_{\rm peak}}{x} \exp\left[-\gamma\left(\frac{M_{I_2}}{M_{H_2}}\right)^{1/2} E_{\rm th}^2\{x-1\}^q\right]. \tag{12}$$

Using the DEA cross sections for H_2 only, we can obtain the two fitting parameters γ and q for the excited $^2\Sigma_g^+$ resonant state. The values of these two parameters are $\gamma = 0.328\,28$ eV^{-2} and $q = 1.5087$. Using different values of $\sigma_{\rm peak}$, $E_{\rm th}$, and the ratio M_{I_2}/M_{H_2} from Table I, and the values of parameters γ and q, the DEA cross sections for all the isotopes of H_2 can be obtained for any value of electron energy. The calculated and fitted—via Eq. (12)—DEA cross sections are compared in Fig. 2 for the excited $^2\Sigma_g^+$ intermediate resonant

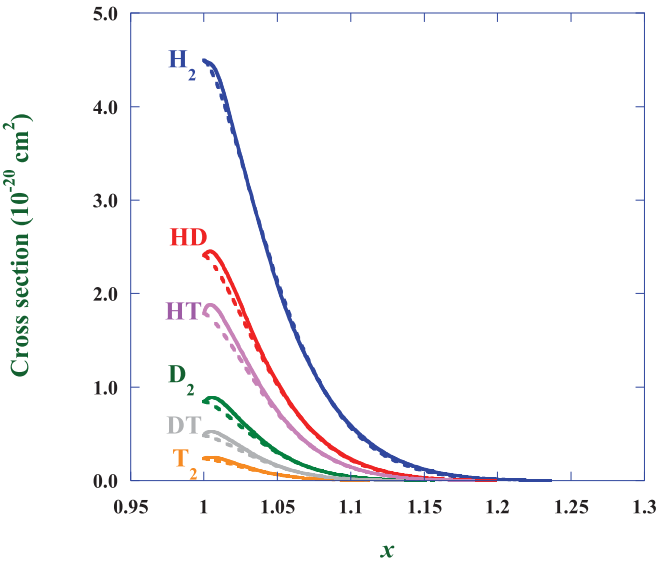

FIG. 2. (Color online) Cross sections for the DEA process occurring through the Rydberg $^2\Sigma_g^+$ resonant state, for all isotopes of H_2, as a function of $x = E/E_{th}$. Full lines: calculated cross sections; dashed lines: fitted cross sections obtained from Eq. (12).

state. A good agreement between the two cross sections indicates that the fitting provided by Eq. (12) is not only simple but also quite accurate.

III. RATE COEFFICIENTS

Kinetic modeling of hydrogen plasmas requires the rate coefficients for the considered processes rather than their cross sections. In this section we present the rate coefficients $K(T)$, as function of electron temperature T, for the process (1) occurring through the excited Rydberg $^2\Sigma_g^+$ resonant state. Also, we will provide an analytical fit and a mass scaling of the rate coefficients derived from the equations of the previous section.

The general expression for $K(T)$, once a Maxwellian energy distribution function is assumed for the electrons, is given by

$$K(T) = \sqrt{\frac{8}{m_e \pi}} \left(\frac{1}{kT}\right)^{3/2} \int_0^\infty dE\, E e^{-\frac{E}{kT}} \sigma(E). \quad (13)$$

Making use of Eq. (10) for $\sigma(E)$, replacing the lower limit of the integral by E_{th} (σ vanishes for E below E_{th}), and introducing the variable $u = (E - E_{th})/kT$, the rate coefficient becomes

$$K_{I_2}(T) = \sqrt{\frac{8}{m_e\, \pi\, kT}} \sigma_{peak} e^{-E_{th}/kT} E_{th} \times \int_0^\infty du\, e^{-u} e^{-\alpha^2 u^2/4}, \quad (14)$$

where $\alpha^2 = 4\gamma\, (M_{I_2}/M_{H_2})^{1/2} k^2 T^2$ is a dimensionless quantity. In this formula σ_{peak}, E_{th}, and α refer to the specific isotope I_2.

The integral on the right-hand side can be expressed in terms of the error function $\Phi\,(1/\alpha)$ [17] as

$$K_{I_2}(T) = \sqrt{\frac{8}{m_e kT\alpha^2}}\, \sigma_{peak} E_{th} e^{-\left[\frac{E_{th}}{kT} - \frac{1}{\alpha^2}\right]} \left[1 - \Phi\left(\frac{1}{\alpha}\right)\right]. \quad (15)$$

Using the first terms in the expansions of the complementary error function $[1 - \Phi(1/\alpha)]$ for small and large values of the argument $1/\alpha$, namely [17],

$$[1 - \Phi(1/\alpha)] = 1 + O(1/\alpha), \quad 1/\alpha \ll 1, \quad (16)$$

$$[1 - \Phi(1/\alpha)] = (\alpha/\pi^{1/2}) \exp(-1/\alpha^2)[1 + O(\alpha^2)], \quad 1/\alpha \gg 1, \quad (17)$$

one obtains from Eq. (15)

$$K_{I_2}(T) = \sqrt{\frac{2}{m_e \gamma}} \left(\frac{M_{H_2}}{M_{I_2}}\right)^{1/4} \left(\frac{1}{kT}\right)^{3/2} \sigma_{peak} E_{th} e^{-\frac{E_{th}}{kT}}, \quad kT \gg 1 \text{ eV} \quad (18)$$

and

$$K_{I_2}(T) = \left(\frac{8}{m_e \pi}\right)^{1/2} \left(\frac{1}{kT}\right)^{1/2} \sigma_{peak} E_{th} e^{-\frac{E_{th}}{kT}}, \quad kT \ll 1 \text{ eV}. \quad (19)$$

From Eqs. (18) and (19) we see that the temperature dependence of rate coefficient for $kT \gg 1$ eV and $kT \ll 1$ eV is quite different [$\sim T^{-3/2} \exp(-\text{const}/T)$ and $\sim T^{-1/2} \exp(-\text{const}/T)$, respectively]. Another difference in the behavior of $K(T)$ in these two limits is the absence of the $(M_{H_2}/M_{I_2})^{1/4}$ factor in Eq. (19). This fact, however, has little significance for the isotope effect since the main mass dependence of $K(T)$ is contained in σ_{peak} (see Table I).

From the ratio K_{I_2}/K_{H_2} expressions can be drawn to obtain mass-scaling relations for the rate coefficients for $kT \gg 1$ eV and $kT \ll 1$ eV in the form

$$K_{I_2}(T) = K_{H_2}(T) \frac{\sigma_{peak}(I_2)}{\sigma_{peak}(H_2)} \left(\frac{M_{H_2}}{M_{I_2}}\right)^{1/4} e^{-(E_{th_{I_2}} - E_{th_{H_2}})/kT}, \quad kT \gg 1 \text{ eV}, \quad (20)$$

$$K_{I_2}(T) = K_{H_2}(T) \frac{\sigma_{peak}(I_2)}{\sigma_{peak}(H_2)} e^{-(E_{th_{I_2}} - E_{th_{H_2}})/kT}, \quad kT \ll 1 \text{ eV}, \quad (21)$$

where we have set $E_{th_{I_2}}/E_{th_{H_2}} \approx 1$ in the preexponential factors. A general scaling relation, valid for any value of kT, can be obtained from Eq. (15) but will have a more complicated structure and contain the difference of error functions.

Equations (20) and (21) allow to calculate $K_{I_2}(T)$ in the regions $kT \gg 1$ eV and $kT \ll 1$ eV for any isotope I_2 once the rate coefficient for hydrogen $K_{H_2}(T)$ is known. All other necessary quantities are given in Table I. We have calculated $K_{H_2}(T)$ numerically and then fitted by adopting the simple expression

$$K_{H_2}(T) = c_1 \frac{e^{-E_{th}/kT}}{(kT)^{1/2} + c_2\, (kT)^{3/2}} \quad (22)$$

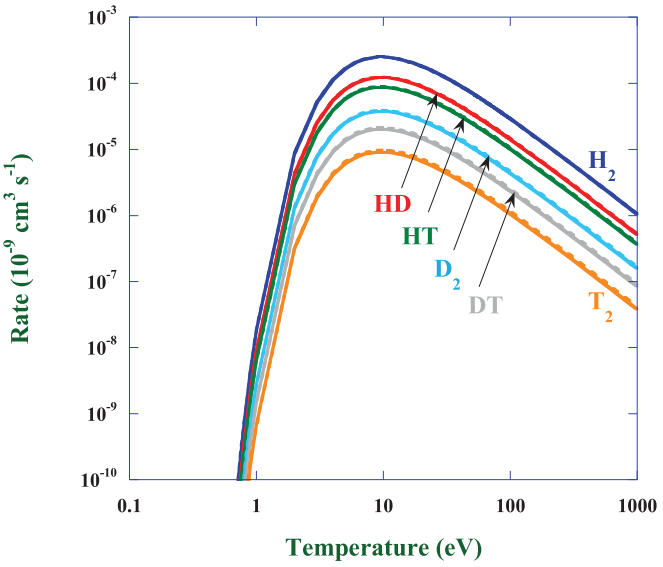

FIG. 3. (Color online) Rate coefficients as function of temperature T, in eV units, for the DEA process occurring through the $^2\Sigma_g^+$ excited electronic resonant state for all isotopes of H_2. Full lines: calculated rates; dashed lines: fitted rates for H_2 [Eq. (22)] and scaled rates for the other isotopes [Eq. (20) for $T \geqslant 1$ eV and Eq. (21) for $T < 1$ eV].

that has a high- and low- temperature behavior consistent with Eqs. (18) and (19). The fitting coefficients c_1 and c_2 are $c_1 = 0.0566\,28$ cm^3 s^{-1} eV$^{1/2}$ and $c_2 = 1.6858$ eV^{-1}. The accuracy of the fit (22) for the H_2 rate coefficients is within ∼0.0003%–4% in the kT range 0.5–500 eV for the $^2\Sigma_g^+$ resonance.

In Fig. 3 are shown the rate coefficients for the DEA process involving the excited $^2\Sigma_g^+$ Rydberg resonant state calculated numerically from Eq. (13) (full lines) and those (dashed lines) obtained by using Eq. (22) and the mass-scaling expressions Eqs. (20) and (21), for the high and low temperatures, respectively, for the other isotopes.

In presenting the scaled curves in Fig. 3 we used Eq. (20) for $kT \geqslant 1$ eV and Eq. (21) for $kT < 1$ eV. Due to their asymptotic nature, these two equations are not expected to merge smoothly at the "separation point" of 1 eV. At this temperature, in fact, a discontinuity in the rates is expected, generated by the factor $(M_{H_2}/M_{I_2})^{1/4}$ present only in Eq. (20). This factor introduces a "mismatch" of the two asymptotics at $kT = 1$ eV of 24% for T_2, which for HD becomes 7%. This discontinuity however, is not evident in the plots of Fig. 3 due to the logarithmic scale. For the lighter isotopes the same factor is closer to the unity and so is even less apparent.

The accuracy for the scaled rates for the Rydberg resonance ranges from 0.07%–7% in the interval 1–1000 eV. The worst case is represented by the T_2 molecule. Immediately below 1 eV the scaling accuracy strongly deteriorates as the electron temperatures approach 0.1 eV, reaching the value of ∼20% for all the isotopes. This could be more due to the numerical uncertainty of the original data having too small values rather than to the analytic expressions (20)–(22) which have the correct asymptotic behavior both at high and low kT.

We have observed from our calculations that Eq. (20) shows a good accuracy also below 1 eV, even better than that of Eq. (21), at least for not too low temperatures where Eq. (15) should be used. This is probably due to the fact that in the ratio $K_{I_2}(T)/K_{H_2}(T)$ the term $\exp(1/\alpha^2)[1 - \Phi(1/\alpha)]$ is more or less independent of the mass, so it cancels in the ratio leading again to expression (20), which now is valid for a larger range of temperatures, above and below the separation point. For very low temperatures, say, below 0.1 eV, Eq. (21), however, is expected to give the more realistic results.

For the Rydberg $^2\Sigma_g^+$ resonant state the rate coefficients, shown in Fig. 3, increase as the electron temperature is raised up to their maximum value K_{max} at some temperature T_{max} before falling off with increasing temperature. The value of T_{max} increases with increasing mass of the isotopes. By differentiating Eq. (18) one obtains $kT_{max} = 2E_{th}/3$, which is consistent with the values of E_{th} in Table I and the location of the maximum value of the rate coefficients in Fig. 3. Furthermore, the maximum value of the rate coefficient K_{max} for each isotope is determined by the peak value of the DEA cross sections, which are also listed in Table I.

The main focus of the present work is on the DEA process for H_2 and its isotopes involving the Rydberg $^2\Sigma_g^+$ resonance. For the sake of comparison, however, we also look at the DEA cross sections and rates, for all isotopes of H_2, involving the $X^2\Sigma_u^+$ shape resonance which are available in previous papers [18,19]. The isotope effect is much more pronounced for the case involving the $X^2\Sigma_u^+$ shape resonance than the case involving the Rydberg $^2\Sigma_g^+$ resonance. In the first case it spans five orders of magnitude in the temperature region about the peak values and above when going from H_2 to T_2, while in the second case this span is only a factor of 10. This is a consequence of the large difference of the local widths of the two resonances at $R = R_0$. It should be noted that the peak value of the DEA rate coefficients for hydrogen involving the Rydberg $^2\Sigma_g^+$ resonance is ∼10 times larger than the corresponding peak of the rate coefficient involving the $X^2\Sigma_u^+$ resonance. This factor increases to 100 when HD is considered, and to $\sim 10^5$ in the T_2 case. This indicates that the DEA process proceeding via the Rydberg $^2\Sigma_g^+$ resonance is much faster than when it proceeds via the $X^2\Sigma_u^+$ resonance, its efficiency increasing dramatically with the increase of reduced mass of the isotopes. For $kT \approx 2$ eV, for instance, the DEA rate coefficients for H_2 in the two resonant states are of the same order of magnitude, while those for T_2 differ by four orders of magnitude. Because of the large value of the threshold energy in the exponent of Eq. (22) in the case of $^2\Sigma_g^+$ Rydberg resonance, the corresponding rate coefficients decrease very rapidly with decreasing the temperature. Thus, already for $T \approx 0.5$ eV, the DEA rate coefficients for H_2 and T_2 involving the $X^2\Sigma_u^+$ resonance are $\sim 10^8$ and 10^4 times larger than those involving the Rydberg $^2\Sigma_g^+$ resonance. The DEA rate coefficients involving the Rydberg $^2\Sigma_g^+$ resonance become competitive with those involving the $X^2\Sigma_u^+$ resonance at ∼1 eV for T_2 and ∼2 eV for H_2, and at higher temperatures the DEA via the Rydberg $^2\Sigma_g^+$ resonance becomes the dominant process. This may be the case in some astrophysical or laboratory plasmas, such as the interstellar medium and edge plasmas of magnetic fusion devices. We note that the dominance of DEA via the Rydberg $^2\Sigma_g^+$ resonance over that proceeding via the $X^2\Sigma_u^+$ resonance

is also maintained up to $T = 10$ eV when the H_2 molecule is in the $v = 1$ and $v = 2$ vibrational levels [20].

IV. DISCUSSION AND CONCLUSIONS

From the one dimensionality (one nuclear coordinate) of nuclear motion involved in the DEA process considered in this paper and from the adopted WKB approximation in deriving the analytical form of its cross section [Eqs. (2) and (3)], it is obvious that Eq. (12) for the scaled cross section is valid also for the $X^2\Sigma_u^+$ and $B^2\Sigma_g^+$ resonances of H_2. For instance, for the $X^2\Sigma_u^+$ resonance, the parameters γ and q of Eq. (12) have the values 0.545 76 eV^{-2} and 1.1937, respectively, not too different from their values for the Rydberg $^2\Sigma_g^+$ resonance. For the same reason, Eq. (12), in its general form, should be valid also for the isotopes of any diatomic molecule, provided the local-complex-potential (LCP) model for the resonant scattering is applicable. Thus, a significant isotope effect has been observed [21] in DEA in HCl and DCl systems (the $H + Cl^-$ cross-section peak being approximately five times larger than that for $D + Cl^-$), but the nonlocal effects in the process prevent its description by the simple LCP WKB version of the process [22]. We also mention that the thermal averaged (at 300 K) DEA cross sections for HCl/DCl, HBr/DBr, and HI/DI systems, calculated within the nonlocal resonant theory [23], show that the ions Cl^-, Br^-, and I^- are produced more effectively by a factor of 7, 5.7, and 2.15, respectively, in the case of the lighter isotope.

In the case of polyatomic systems, with many modes of nuclear motion, the dynamics of DEA process is quite different from that in the diatomic case [24]. Some of the vibration modes in a polyatomic molecule may exhibit Fermi resonances when the two-dimensional nuclear motion cannot be separated. Furthermore, the resonant states have complex potential energy hypersurfaces that may be coupled by nonadiabatic or Renner-Teller couplings. Finally, the number of DEA channels in a polyatomic molecule can be large. Within a multidimensional WKB approach (and the LCP model) one can still separate the electron capture event and the DEA nuclear evolution [as in Eq. (2)], and for a selected mode of nuclear motion (in the absence of a Fermi resonance between this mode and another mode) one can even generalize Eq. (3) for the capture cross section. However, a single reduced-mass factor cannot be extracted in explicit form in the exponent of Eq. (2) if two or more resonant states are coupled. The full complexity of nuclear dynamics has been demonstrated [25] on the simple three-atom system, H_2O, involving the complex potential energy surfaces of $^2B_1$, $^2A_1$, and $^2B_2$ resonant states and using the multiconfiguration time-dependent Hartree method. The isotopic effect in the $H^- + OH$ DEA channel (H substituted by D) has also been studied, revealing that the process when proceeding via any of the above resonances exhibits a cross-section peak for the $D^- + OD$ production slightly higher than that for $H^- + OH$. This is in contrast with the expectation based on the single-mode result, Eq. (12), but for the channel proceeding via the $^2B_1$ resonance (which decays mainly by autodetachment) this finding is consistent with the experimental observations [26]. It should be remarked, however, that in an earlier experiment [27] the ratio of DEA cross-section peaks for $D^- + OD$ and $H^- + OH$ production via the $^2B_1$ resonance of water was found to be 0.75.

Interpreted as a relation of the DEA cross section with the reduced mass of dissociation products, the single-mode results, Eq. (8) or Eq. (10) (written in general form), may still reflect the dissociation dynamics in certain classes of polyatomic molecules when one anion is preferentially produced. This is the case with the n-$C_nH_{2n+1}Br$ class of molecules in which the $Br^- + n$-C_nH_{2n+1} dissociation channel is dominant. The measured DEA cross sections for this channel for $n = 2$–6, 8 all exhibit peaks at ~0.7 eV whose ratios are consistent with the single-mode relation (9) [28]. Additional examples of DEA in polyatomic systems, where the single-mode description can be useful in the interpretation of reduced-mass dependence of experimentally observed DEA cross-section peaks, can be found in Ref. [29]. However, in the general case, the complexity of the DEA process in polyatomic systems remains high and still not properly explored.

To conclude, in the present paper we have reported calculations of cross sections for dissociative electron attachment, to H_2 and all its heavier isotopic variants, occurring through the Rydberg $^2\Sigma_g^+$ resonant state. A careful analysis, based on the WKB formulation of the resonant processes, leads to an effective fitting expression for the cross sections for H_2 and to a simple mass-scaling law which allows for an accurate evaluation of the cross sections for the heavier isotopes. Rate coefficients are also calculated for the DEA processes occurring through this resonance. Again, an analytical fitting expression for the rate coefficients, derived from the WKB representation of the cross sections, has been obtained for H_2 as a function of the electron temperature. Asymptotic mass-scaling laws have been finally established which accurately reproduce the calculated rates for the heavier isotopes and allow for a reliable extrapolation beyond the range of electron temperatures considered here.

ACKNOWLEDGMENT

The research leading to these results has received funding from the European Community's Seventh Framework Program (FP7/2007-2013) under Grant agreement No. 242311.

[1] S. Lepp, P. C. Stancil, and A. Dalgarno, J. Phys. B **35**, R57 (2002).
[2] *Atomic and Molecular Processes in Fusion Edge Plasmas*, edited by R. K. Janev (Plenum, New York, 1995).
[3] J. N. Bardsley and F. Mandl, Rep. Prog. Phys. **31**, 471 (1968).
[4] D. Rapp, T. E. Sharp, and D. D. Briglia, Phys. Rev. Lett. **14**, 533 (1965).
[5] G. J. Schulz, Phys. Rev. **113**, 816 (1959).
[6] G. J. Schulz and R. K. Asundi, Phys. Rev. Lett. **15**, 946 (1965).
[7] G. J. Schulz and R. K. Asundi, Phys. Rev. **158**, 25 (1967).

[8] J. N. Bardsley, A. Herzenberg, and F. Mandl, Proc. Phys. Soc. London **89**, 321 (1966).
[9] G. V. Dubrovskii, V. D. Ob'edkov, and R. K. Yanev, Theor. Exp. Chem. **3**, 361 (1967).
[10] T. F. O'Malley, Phys. Rev. **150**, 14 (1966).
[11] R. Celiberto, R. K. Janev, J. M. Wadehra, and A. Laricchiuta, Phys. Rev. A **80**, 012712 (2009).
[12] J. N. Bardsley, A. Herzenberg, and F. Mandl, in *Atomic Collision Processes*, edited by M. R. C. McDowell (North-Holland, Amsterdam, 1964), p. 415.
[13] Yu. N. Demkov, Phys. Lett. **15**, 235 (1965).
[14] E. Merzbacher, *Quantum Mechanics*, 3rd ed. (Wiley, New York, 1998).
[15] R. Celiberto, R. K. Janev, J. M. Wadehra, and A. Laricchiuta, Phys. Rev. A **77**, 012714 (2008).
[16] J. M. Wadehra, Proc. SPIE **1061**, 522 (1989).
[17] I. S. Gradshteyn and I. M. Ryzhik, *Table of Integrals Series and Products* (Academic, San Diego, CA, 2000).
[18] R. Celiberto, R. K. Janev, A. Laricchiuta, M. Capitelli, J. M. Wadehra, and D. E. Atems, At. Data Nucl. Data Tables **77**, 161 (2001).
[19] J. M. Wadehra, Appl. Phys. Lett. **35**, 917 (1979).
[20] R. Celiberto, R. K. Janev, J. M. Wadehra, and J. Tennyson, Chem. Phys. (in press).
[21] R. Azria, L. Roussier, R. Paineau, and M. Tronc, Rev. Phys. Appl. (Paris) **9/2**, 469 (1974).
[22] J. N. Bardsley and J. M. Wadehra, J. Chem. Phys. **78**, 7227 (1983).
[23] K. Houfek, M. Čižek, and J. Horáček, Phys. Rev. A **66**, 062702 (2002).
[24] T. N. Rescigno, C. W. McCurdy, D. J. Haxton, S. C. Trevisan and A. E. Orel, J. Phys.: Conf. Ser. **88**, 012027 (2007).
[25] D. J. Haxton, T. N. Rescigno, and C. W. McCurdy, Phys. Rev. A **75**, 012711 (2007).
[26] J. Fedor, P. Cicman, B. Coupier, S. Feil, M. Winkler, K. Gluch, J. Husarik, D. Jaksch, B. Farizon, N. J. Mason. P. Scheier and T. D. Märk, J. Phys. B **39**, 3935 (2006).
[27] R. N. Compton and L. G. Christophorou, Phys. Rev. **154**, 110 (1967).
[28] L. G. Christophorou, J. G. Carter, P. M. Collins, and A. A. Christodoulides, J. Chem. Phys. **54**, 4706 (1971).
[29] L. G. Christophorou, Environ. Health Perspect. **36**, 3 (1980).